Rapid Detection of Ag (I) via Size Induced Photoluminescence Quenching of Biocompatible Green Emitting L-Tryptophan Scaffolded Copper Nanocluster

Aarya,[1] Telna Thomas,[1] Bibhu Ranjan Sarangi[2,3] and Supratik Sen Mojumdar[1]*

[1]Department of Chemistry, Indian Institute of Technology Palakkad, Kerala, India – 678 557
[2]Department of Physics, Indian Institute of Technology Palakkad, Kerala, India – 678 557
[3]Department of Biological Sciences and Engineering, Indian Institute of Technology Palakkad, Kerala, India – 678 557

Abstract

Atomically precise metal nanoclusters capped with small molecules like amino acids are highly favoured due to their specific interactions and easy incorporation into biological systems. However, they are rarely explored due to the challenge in surface functionalization of nanocluster with small molecules. Herein, we report the synthesis of green emitting (λ_{ex} = 380 nm, λ_{em} = 500 nm) single amino acid (L-tryptophan) scaffolded copper nanocluster (Trp-Cu NC) via one-pot route under mild reaction conditions. The synthesized nanocluster can be used for the rapid detection of heavy metal (Ag(I)) in the nanomolar concentration range in real environmental and biological samples. The strong green photoluminescence intensity of the nanocluster quenched significantly upon addition of Ag(I) due to the formation of bigger nanoparticles, thereby losing its energy quantization. A notable colour change from light yellow to reddish brown can also be observed in the presence of Ag(I) allowing its visual colorimetric detection. Portable paper strips fabricated with Cu-Trp NC can be reliably used for on-site visual detection of Ag(I) in the micromolar concentration range. The Trp-Cu NC possesses excellent biocompatibility making them suitable nanoprobe for cell imaging, thus can act as an in-vivo biomarker. The nanocluster showed a significant spectral overlap with an anticancer drug doxorubicin, thus can be used as an effective FRET pair. FRET results can reveal important information regarding the attachment of the drug to the nanocluster and hence, its role as a potential drug carrier for targeted drug delivery within human body.

Keywords: Copper Nanocluster, Metal Sensor, Photoluminescence, Biocompatible, Cell Imaging, FRET

---

*Email: supratik@iitpkd.ac.in

Introduction

Ligand protected noble metal nanoclusters (e.g. Au, Ag, Cu etc.) emerged as an efficient nanoprobe grabbing a lot of recent interest owing to their luminescence properties, ease of synthesis, low cytotoxicity, photostability and biocompatibility [1–7]. These nanoclusters with their improved physicochemical and optical properties have broad applicability in sensing [8, 9], catalysis[3, 10], bioimaging [9, 11] and therapeutics [12–14]. Metal nanoclusters are ultra-small sized particles comprising several to tens of atoms [6, 15–17]. Their extraordinary photophysical properties are associated with the presence of quantized and discrete energy levels due to their small size (< 2 nm) [15–17]. Despite the natural abundance, copper nanoclusters have been less explored compared to Au and Ag. Due to its relatively higher oxidation potential it is challenging to reduce copper and once formed the copper nanocluster can readily undergo oxidative damage [17–19].

In protein capped metal nanoclusters, small amino acids like tryptophan and tyrosine play a crucial role in protecting the nanocluster by coordinating with the metal core as well as reducing the metal ions [18–21]. Thus one might anticipate that the individual amino acids can also play a similar role outside the protein structure forming a stable ultrasmall nanocluster without the involvement of a large macromolecule, where the surface properties can be easily tuned. The bidentate carboxylate group and the lone pair of electrons of the amino group of the individual amino acids are promising for protecting nanocluster ensuring better metal coordination and specific interaction [5]. Small molecule templated nanoclusters can be easily incorporated within a biological system such as live cell [20, 22] but surface functionalization of metal nanoclusters with small molecules as the capping agent is challenging [20].

L-Tryptophan, one of the eight essential amino acids, is the only precursor for synthesizing melatonin and serotonin. Serotonin is an important neurotransmitter and neuromodulator responsible for regulating mood, behaviour and cognition whereas melatonin acts as a regulator of sleep/wake rhythms and reduces oxidative stress [23, 24]. In the liver, tryptophan is converted to niacin (Vitamin B3) which has many essential biological functions such as energy metabolism, DNA synthesis etc [25, 26]. It is primarily found in transmembrane proteins. It helps anchor the membrane proteins with the cell membrane [27, 28]. It has a high affinity to transport across the blood-brain barrier compared to other amino acids [28] and thus could act as a potential drug carrier. Although it is found in the lowest concentration in the body, it is a critical component in protein synthesis and essential metabolic pathways [23]. Tryptophan templated copper nanoclusters thus could be a suitable nanoprobe for in-vivo studies.

Silver, a noble and precious metal, has been extensively used in various fields such as medicines [29], drug delivery [30], textiles [31], jewellery, catalysis [32] and electronics [33]. The antimicrobial

property of Ag(I) has been explored in water purification and therapeutic applications [29, 34]. But the unconstrained release of Ag (I) (a heavy metal) into the environment as a part of many anthropogenic activities and rapid industrial growth has led to a significant increase in their concentration in the environment (especially in water resources) resulting in adverse effects on human health and environment [35]. Once they enter into the body, they can accumulate and deposit resulting in many adverse health disorders [35, 36]. Commonly high concentrations of Ag (I) in the human body can lead to skin discoloration causing Argyria [37, 38]. The interaction of Ag (I) with thiol groups can lead to the inhibition of the enzymatic activity of proteins [39, 40]. Due to its binding affinity towards purine and pyrimidine bases in DNA, silver ions and silver nanoparticles can damage the DNA [41]. Apart from genotoxicity, it has also been found to induce renal, hepatic and neurological toxicities [37]. It can displace important metal ions like Ca^{2+} and Zn^{2+} in hydroxyapatite in bone [42]. Thus it is essential to detect Ag(I) in biological and environmental systems with high sensitivity and selectivity. However, till date, sensors for rapid and selective detection of Ag (I) ions are limited, most of the cases involving complex mechanisms or instrumentations [43, 44]. This calls for the need of a simple, reliable, robust, sensitive, water soluble, biocompatible, cost-effective, time efficient and highly selective sensor for the ultrasensitive detection of Ag (I).

Traditionally available sophisticated analytical techniques commonly used for the detection of Ag (I) involve Atomic Absorption/Emission Spectrometry (AAS/AES) [45], Inductively Coupled Plasma Atomic-Emission Spectrometry (ICP-AES) [46], Mass spectrometry (ICP-MS) [47], Surface Enhanced Raman Spectroscopy (SERS) [48] etc. Even though detection limits of some of these techniques can reach up to 0.1 nM, they are less favoured as they are costly, require cumbersome sample preparation, complicated and sophisticated instrumentation, complex detection process and trained personnel [49]. Fluorescent probes on the other hand are more favoured as sensors as they are rapid and user friendly [50, 51]. Various fluorescent probes have been developed as sensors for Ag(I) using organic templates [52], quantum dots [53] and nanoparticles [39, 43, 54]. The detection method is rapid and sensitive but they too suffer from one or more drawbacks, either they are insoluble in water [55, 56] or, highly toxic for the human body [57]. Thus the development of fluorescence based biocompatible optical sensors with desirable features is in high demand. Ligand protected metal nanoclusters thus could be a better choice for the selective detection of Ag(I). Most recently researchers attempted to develop metal nanoclusters for detection of Ag(I) [58–61] but they too need improvements since the limit of detection were high and the cytotoxicity for these nanoclusters has not been checked, thus could pose threat to human health.

Here we report a protocol for the synthesis of green-emitting L-tryptophan stabilized ultrasmall (diameter ~2 nm) copper nanocluster (Trp-Cu NC) which can rapidly and selectively detect Ag (I) in the nanomolar concentration range (detection limit ~25 nM) in complex systems such as real water

samples and human serum. The Trp-Cu NC was found to be highly photostable, biocompatible and have better quantum yield (ϕ = 0.114) than the previously reported work [62]. It has a significant spectral overlap with an anticancer drug (doxorubicin) making it a suitable candidate for a FRET-pair to study the drug binding/release. The synthesized Trp-Cu NC can be used as a nanoprobe for cell imaging and intracellular studies making it a suitable candidate for in vivo biomarkers. The ability of tryptophan to engage in multiple types of interactions and its role in membrane protein stabilization makes the internalization of NC easier for in vivo studies. Thereby it opens up its potential application as a drug delivery agent.

Materials and Methods

Materials

L-Tryptophan was purchased from Sisco Research Laboratories Pvt. Ltd. (SRL). Copper chloride ($CuCl_2.2H_2O$), sodium hydroxide (NaOH) and hydrazine hydrate (N_2H_4) used for the synthesis of Cu-Trp NC were purchased from Nice Chemicals (NICE). The following metal salts for examining metal ion sensing of NC were purchased either from SRL or NICE: mercuric chloride ($HgCl_2$), silver nitrate ($AgNO_3$), calcium chloride ($CaCl_2$), sodium chloride (NaCl), magnesium chloride ($MgCl_2$), manganese chloride ($MnCl_2$), nickel sulphate ($NiSO_4$), cadmium chloride ($CdCl_2$), chromic nitrate [$(Cr(NO_3)_2$], ferrous chloride ($FeCl_2$), lead nitrate [$Pb(NO_3)_2$], cobalt nitrate [$Co(NO_3)_2$], zinc sulphate ($ZnSO_4$), sodium arsenate (Na_2HAsO_4) and nickel sulphate ($NiSO_4$). Hydrogen peroxide (H_2O_2), sodium hypochlorite (NaOCl) solution and concentrated hydrochloric acid (HCl) were purchased from Nice chemicals. L-Cysteine was purchased from SRL. Quinine hemi-sulphate dye and human serum were purchased from sigma-aldrich. Doxorubicin hydrochloride for FRET studies was purchased from TCI (Tokyo Chemical Industry) chemicals. Double distilled water from Biopak Polisher Milli-Q water system (CDUFB1001) was used for preparing all the solutions. All the reagents were used as received as without any further purification.

Synthesis of L-Tryptophan scaffolded Copper nanocluster

To synthesize L-tryptophan scaffolded copper nanocluster (Trp-Cu NC), 1 ml of 0.15 mM $CuCl_2$ was added to 2 ml of 7.5 mM L-Tryptophan solution in a 1:100 (Cu:Trp) molar ratio. The reaction mixture was vigorously stirred at 40^{o}C for half an hour. This was followed by dropwise addition of 100 µl of 1 M NaOH to adjust the pH of the solution to 12. After half an hour of stirring, 50 µl of 80% hydrazine hydrate was added dropwise to the reaction mixture. The solution was then kept for vigorous stirring at 40 ^{o}C for 8 hrs (Scheme 1a). The formation of NC was indicated by the appearance of a yellowish brown coloured transparent solution which turned into green under UV light (Scheme 1b). After completion of the reaction, the sample was stored at 4^{o}C under dark condition for further use.

Instrumentation

Steady state fluorescence measurements were recorded using Perkin Elmer Fluorescence Spectrometer (FL 8500). The L-tryptophan scaffolded Cu NC solution was excited at 380 nm and the spectra were scanned from 390 nm to 700 nm at a scan speed of 240 nm min^{-1} keeping excitation and emission slit widths at 5 nm with 430 nm emission filter. Life time measurements were done on a time-correlated single photon counting setup (LifeSpec-II, Edinburgh Instruments, UK) using a 375 nm pulsed diode laser with an instrument response function of 150 ps. The size of the NC was determined using High Resolution Transmission Electron Microscope (HRTEM) from JEOL Japan (model no. JEM-2100 Plus). The sample was drop casted on a carbon coated copper grid. Fourier transform infrared (FTIR) spectra were recorded using IR Tracer-100 FTIR spectrophotometer from Shimadzu Scientific Instruments scanning in the wavenumber range of 7800-350 cm^{-1} at 0.2 cm^{-1} resolution. For Matrix Assisted Laser Desorption/Ionisation – Time of Flight (MALDI-TOF) mass spectrometry analysis, a Bruker make Ultraflextreme MALDI-TOF analyser was used with trans-2-[3-(4-tert-Butylphenyl)-2-methyl-2-propenylidene]malononitrile (DCTB) as the matrix. Inductively Coupled Plasma-Optical Emission Spectrometry (ICP-OES) measurements were done using the Perkin Elmer Optima 5300 DV instrument for quantitative determination of Ag(I) in real samples. The photoluminescence quantum yield (ϕ) of the nanocluster was measured using the method reported earlier [63].

Metal sensing studies

For the metal sensing studies, the diluted solution of Trp-Cu NC (~25 times) was incubated with desired concentration of different metal cations (Cd^{2+}, Cr^{3+}, Fe^{2+}, Ni^{2+}, Co^{2+}, Zn^{2+}, Hg^{2+}, As^{5+}, Mn^{2+}, Na^{+}, K^{+}, Ca^{2+}, Mg^{2+}, Pb^{2+} and Ag^{+}) for ~3 mins prior to the measurement. To test the sensitivity, increasing concentration of Ag^{+} (25 nM – 500 µM) were added to 1 ml of diluted NC and emission spectra were recorded after 3 min of incubation after each addition. Reported errors represent standard error on mean (s.e.m) calculated from at least three or more independent measurements.

Fluorometric analysis of Ag(I) with Trp-Cu NC coated paper strips

Whatman filter paper was cut into pieces in circular shape and immersed into Cu-Trp NC solution. After 10 minutes, it was removed and air dried at room temperature. 10 µl of different concentrations of Ag(I) (5 µM, 25 µM, 50 µM, 100 µM, 500 µM and 1000 µM) were then drop-casted on the paper strips coated with NC and observed under UV lamp.

Detection of Ag(I) in real samples

The prepared NC was applied to estimate Ag(I) in real specimens like tap water and human serum. Various concentrations of Ag(I) (500 nM, 50 µM and 100 µM) were spiked into 1 ml of the NC solution containing 100 µl of real specimens. After 3 mins of incubation the emission spectra were recorded.

Cell Viability and Imaging

The cell viability studies were done following MTT based assay mentioned earlier [63]. Briefly, the 3T3 (normal mouse fibroblast) cells were incubated with varying concentrations (1 to 80 μM) of Trp-Cu nanocluster for 24 hours. After incubation MTT was added to each well (final concentration ~ 0.5 mg/ml). The resulting formazan crystals were dissolved in DMSO and absorbance was recorded in a plate reader (Biotech Epoch 2NS Gen5) at 590 nm using a 620 nm reference filter. Normalized viability and s.e.m was calculated from at least three independent measurements done for each concentration. For imaging the cells were incubated with 20 μM Trp-Cu nanocluster for 6 hours. Post incubation cells were fixed using para formaldehyde. Imaging was done using confocal microscope (Olympus fluoview fv3000) with suitable excitation (λ_{ex} = 405 nm) and emission parameters.

Fluorescence Resonance Energy Transfer (FRET):

FRET efficiency (E_{FRET}) can be calculated using the equation [64]:

$$E_{FRET} = 1 - \frac{I_{DA}}{I_D} \quad (1)$$

where, I_{DA} and I_D are the photoluminescence intensity of the donor in the presence and absence of the acceptor respectively. The Förster distance (R_0) was estimated from the spectral overlap J(λ) using the equations [64]:

$$R_0 = 0.211[\kappa^2 n^{-4} Q_D J(\lambda)]^{\frac{1}{6}} \quad (2)$$

where, κ^2 is the orientation factor (normally assumed as 2/3 for random orientation), n is the refractive index, Q_D is the quantum yield. The overlap integral J(λ) can be measured from the equation below:

$$J(\lambda) = \frac{\int_0^\infty I_D(\lambda)\varepsilon_A(\lambda)\lambda^4 d\lambda}{\int_0^\infty I_D(\lambda) d\lambda} \quad (3)$$

RESULTS AND DISCUSSION

Green Emitting Trp-Cu NC:

The synthesized tryptophan stabilized Cu-NC showed a strong green photoluminescence intensity (λ_{em} ~ 500 nm) with a significant quantum yield (ϕ =0.114) when excited at 380 nm, with a 120 nm Stokes shift (Figure 1). Compared to the negligible emission intensity of pure tryptophan, the strong photoluminescence intensity of Trp-Cu NC indicated that the luminescent properties are intrinsic to the copper nanocluster and not to the tryptophan scaffold (Figure S1). On mixing of Tryptophan and $CuCl_2$ solutions, the nanocluster formation is initiated by the electrostatic interaction between Cu(II) ions and amino and carboxyl groups of tryptophan. Under basic conditions (pH = 12) and in the presence of an external reducing agent, the Cu^{2+} ions get reduced to Cu^0, forming nanocluster by coalescence [62, 65]. The Trp-Cu NC showed excellent photostability for over three weeks when stored at 4°C under dark conditions (Figure S2). In general copper nanoclusters are prone to oxidative damage leading to the

quenching of the photoluminescence intensity [18, 19]. But in the case of Trp-Cu NC absolutely no quenching of the photoluminescence intensity was observed in the presence of strong oxidizing agents like hydrogen peroxide (H_2O_2) and hypochlorite (ClO^-) suggesting that the Trp-Cu nanocluster is highly stable against oxidative damage (Figure S3).

The morphology of the nanoclusters was observed using HR-TEM. TEM image exhibited the existence of monodispersed spherical ultra-small (average size ~ 2 ± 0.1 nm) Trp-Cu nanoclusters (Figure 2). Lattice fringes can also be clearly visible in the TEM image (Figure 2A inset). The interaction between the functional groups of tryptophan and copper in the nanocluster was examined using FTIR. The FTIR spectra of pure tryptophan and Cu-Trp NC showed close resemblance (Figure 3a). The bands around 3000-3400 cm^{-1} corresponds to N-H and O-H stretching vibrations. Indole N-H stretching vibration is observed as a distinctive peak at 3394 cm^{-1}. The band at 1660 cm^{-1} can be assigned to C=O stretching vibration of amide bond. A significant broadening of the bands around 3000-3400 cm^{-1} was observed in the IR spectra of NC due to Cu-N bond formation [65, 66]. This can be attributed to the efficient stabilization of NC by tryptophan.

The precise chemical composition of Cu-Trp NC was successfully assigned by mass spectrometry (MALDI-TOF) technique (Figure 3b). By comparing the spectrum for Trp-Cu NC with that of pure tryptophan, we assigned the observed m/z values to corresponding fragments [62, 67, 68]. The most dominant base peak centred at m/z = 401.495 can be attributed to [Cu_3In+Na^+]. The next most abundant peaks located at m/z = 217.674 and m/z = 467.469 can be assigned to the chemical formula of [$CuIn+Na^+$] and [$Cu_4In+3Na^+$] respectively. Some other less intense peaks are also observed and the respective chemical composition of those nanoclusters are listed in the table S1 [62, 67, 68]. Thus, from the MALDI-TOF analysis, it could be concluded that each tryptophan scaffolded Cu NCs were composed of less than 5 atoms. Although this result deviates from the cluster size predicted by Jellium Model [69, 70], nanoclusters with a lesser number of atoms with emission in the longer wavelength are not uncommon [62, 71, 72].

Selective and sensitive detection of Ag(I)

The strong photoluminescent intensity of Cu-Trp NC can be completely quenched (~ 99%) by 500 μM Ag(I) ions (Figure S4). Based on this remarkable result, an assay was developed for the rapid detection of Ag(I). A series of metal ions (~ 500 μM) were added to the Trp-Cu NC to check the selectivity of the nanocluster towards Ag(I). Only Ag(I) showed significant quenching of the photoluminescence intensity among all the screened metal ions (Figure 4a). Upon addition of Ag(I) (~200 μM), the PL intensity of Trp-Cu NC decreased by ~15 fold (~ 93% quenching) while in the presence of other metal ions (~500 μM) only a minimal change (≤1.5 times decrease) in the PL intensity can be observed, clearly suggesting its selectivity for the detection of Ag(I) (Figure 4a). A significant colour change from pale yellow to reddish brown can also be clearly observed upon the addition of

Ag(I) to the nanocluster solutions. This colour change was not visible for other metal ions, indicating that the Trp-Cu NC can also be used for visual detection of Ag(I) with utmost selectivity (Figure 4b).

Owing to its high reduction potential, Ag(I) can be easily converted to Ag(0) in the presence of any mild reducing agent. Previously small molecules like tryptophan have been assigned as a reducing agent for the reduction of the metal core during the formation of a stable nanocluster [21, 62]. Thus adding Ag(I) to the Trp-Cu NC can undergo a metallophilic interaction with the Cu core followed by a rapid reduction to Ag(0) by tryptophan and hydrazine present in the system. When treated with HCl or, L-cysteine, neither precipitation nor any significant change in the PL intensity was observed suggesting the presence of Ag(0) in the Trp-Cu NC solution. The zero oxidation state of Ag was further confirmed by XPS studies (Figure S5). The Ag(0) then deposited on the surface of the copper NC resulting in an enhancement in the size of the clusters. This increase in the size of Trp-Cu NC after the addition of Ag(I) was confirmed by TEM image (Figure 5). A significant increase in the size (~ 9 fold) from ~2 nm to ~18 nm was observed from the TEM image which distinctly indicates the transition from nanocluster to nanoparticle. The inherent PL property of Trp-Cu NC due to its quantum size was thus lost due to the formation of nanoparticles. This justifies the drastic reduction in the PL intensity of the NC upon the addition of Ag(I) compared to other metal ions.

The sensitivity of the Trp-Cu nanocluster was examined by gradually adding Ag(I) to the nanocluster solution. With increasing concentration of Ag(I) (from nanomolar (~25 nM) to micromolar (~ 500 μM) concentration range) photoluminescence intensity of the nanocluster gradually decreased and completely quenched (~99%) at around ~500 μM Ag(I) concentration (Figure 6a). Interestingly, when F_0/F (where F_0 and F are the PL intensities in the absence and presence of Ag(I) respectively) was plotted as a function of Ag(I) concentration (Intensity based Stern-Volmer Plot) a non-linear curve with upward curvature is observed (Figure 6b), which is a typical characteristic of a combination of static and dynamic quenching mechanism [64, 73]. This plot can be nicely fitted to the following equation containing both the static and dynamic contributions: $\frac{F_0}{F} = (1 + K[Q])e^{V[Q]}$ (Equation 1), where [Q] is the concentration of the quencher, K and V are the dynamic and static quenching constants respectively [73]. Thus the dynamic and static quenching constants ($K = 3.9\times10^4$ M^{-1}, $V = 2.7\times10^3$ M^{-1}) can be obtained readily from the fitted curve. When $\log(F_0/F)$ is plotted against [Ag(I)], a linear fit can be obtained in the concentration range from 0 to 100 μM (Figure 6b inset), which can be further used as a calibration curve ($\log(F_0/F) = 7.8 \times 10^3$ [Q]) for the estimation of Ag(I) in real complex systems. The limit of detection (LOD) for Ag(I) ions was estimated to be 25 nM (Note 1 of supporting info) which is either comparable or better than other sensors for the detection of Ag(I) (Table S2). Our detection limit is well below the permissible amount of silver in the human body and the maximum limit to be present in the drinking water (0.05 mg/L i.e. 0.463 μM) determined by the World Health Organization (WHO) [59].

The lifetime based quenching process is effective in determining the quenching mechanism. Quenching of PL lifetime can only occur due to dynamic/collisional quenching [63, 64]. The average lifetime of Trp-Cu NC in the absence of any quencher is observed to be 5.2 ns (Figure S6a). Upon gradual addition of Ag(I) no significant change in the average lifetime was observed suggesting predominantly a static quenching mechanism (Figure S6b). But upon careful examination a slight but subtle quenching effect can be seen in the ultrafast time scale (< 2 ns) suggesting the possibility of a swift dynamic quenching process (Figure S6c). Thus both static and dynamic quenching can also be manifested from the lifetime measurements.

We have further extended these studies to develop a simple paper strip based sensor for rapid visual detection of Ag(I). The paper strips (Whatman filter paper) were cut in desired shapes, immersed in Trp-Cu NC and airdried at room temperature. When kept under UV light, the strips showed a cyan PL intensity (Figure S7). On addition of different concentrations of Ag(I) (~10 μL), a dark spot was appeared at the centre of the paper strip due to the quenching of the PL intensity. This dark spot intensified with increasing concentration of Ag(I). These results thus suggest that the Trp-Cu NC can be used as a simple, portable, cost effective paper strip based sensor for the rapid quantitative detection of Ag(I) in the micromolar concentration range.

Quantification of Ag(I) in complex samples

To check the applicability and reliability of our sensor in detecting Ag(I) in real-life complex systems, we have chosen tap water and human blood serum as environmentally and biologically relevant samples. Typically the reliability of a sensor is determined by spiking a real sample with a known amount of analyte and subsequently calculating its recovery. In our study we also followed a similar method to check the reliability of the sensor. Initially no Ag(I) was detected in the tap water and the human blood serum. We spiked the complex systems with a known amount of Ag(I) and subsequently estimated the amount of Ag(I) in the samples experimentally using the Trp-Cu NC (Table 1). The values listed in Table 1 suggests that we can estimate and recover the amount of Ag(I) in these complex systems with more than 90% accuracy on average using the Trp-Cu NC. The experimentally obtained results using the synthesized nanocluster as a sensor matched nicely with the values obtained from a standard method using ICP-OES technique (Table 1). The results thus demonstrate that our sensor can be used for rapid and reliable detection of Ag(I) in complex environmentally and biologically relevant samples in the presence of other interferers and analytes.

Cell viability and imaging:

The in-vitro toxicity study of the Trp-Cu NC showed excellent biocompatibility over a wide range of concentrations (Figure 7a). The cells were significantly viable (~ 40 ± 8 %) even at a high concentration (~ 16 μg/ml) of the nanocluster (Figure 7a) suggesting that the nanocluster is non-toxic and can be used

as a biomarker for intracellular studies. The high quantum yield, photostability and non-cytotoxicity make the Trp-Cu NC a suitable nano-probe for cell imaging studies. Upon incubation of the nanocluster with 3T3 cells, high-resolution bright PL images of the cell can be obtained under 405 nm excitation laser using a confocal microscope (Figure 7b), suggesting that the synthesized nanocluster can be used for live-cell imaging. Figure 7b indicates that the nanocluster preferentially localized in the cytosolic region of the cell. The internalization of the nanocluster within the cell takes place through endocytosis which is a fundamental process to internalize molecules through cell membrane [74]. Hypothetically, small scaffolds (eg. amino acids) should easily penetrate the cell membrane compared to their bigger counterparts (eg. proteins) [22], this is exactly what we observed in this study. Compared to Lys-Cu NC [63], L-tryptophan scaffolded nanocluster could easily pass through the cell membrane making it a better nano-probe for cell imaging and other in-vivo studies. Apart from size, better penetration may be explained by the fact that tryptophan can easily attach to the cell membrane [27, 28] thereby making the endocytosis process easier.

Trp-Cu NC: a suitable FRET pair for an anticancer drug

Fluorescence resonance energy transfer (FRET) is an efficient non-radiative energy transfer technique to estimate the distance between two fluorophores (donor and acceptor) in the nano-meter range (<10 nm) [64, 75, 76]. FRET efficiency is extremely sensitive towards distance between the donor and acceptor, and can be easily calculated from the relative fluorescence intensities of the donor in the absence and presence of the acceptor [64, 75, 76]. FRET has been widely used for the study of protein folding [77], DNA and RNA detection [78, 79], interactions of small molecule with an assembly [18, 80] etc. FRET experiments critically depend upon the availability of a suitable FRET pair where the donor emission significantly overlaps with the acceptor absorption [64, 75, 76].

Finding a biocompatible FRET pair for an anticancer drug that can map the in-vivo targeted drug release is extremely challenging. The synthesized Trp-Cu NC showed significant spectral overlap with the anticancer drug Doxorubicin (dox) (Figure 8a) and thus can be used as an effective FRET pair where the nanocluster can act as a donor while the anticancer drug can be used as an acceptor. The Förster distance (R_0) was calculated to be 3.2 nm, lying within the acceptable range for an ideal FRET pair [64]. Upon addition of doxorubicin to the nanocluster, a significant quenching of the photoluminescence intensity of the nanocluster was observed followed by a concomitant increase in the emission intensity of doxorubicin suggesting effective FRET between the NC and doxorubicin (Figure 8b). The corresponding FRET efficiency was calculated to be ~60% with the intermolecular distance of ~2.98 nm between the donor and acceptor. FRET experiments thus can shed important light on the binding and release of the anticancer drug in-vivo thereby opening up the possibility of using the nanocluster as a potent nano-drug carrier for localized and controlled drug release in cancer patients.

Conclusions

We have developed a simple one-pot protocol for the synthesis of ultra-small, photoluminescent and water-soluble L-tryptophan scaffolded copper nanocluster. The synthesized nanocluster with strong green photoluminescent intensity and high quantum yield exhibited drastic quenching of the PL intensity in the presence of Ag(I) ions. Thus, a turn-off PL assay was developed for rapid, selective and sensitive detection of Ag(I) ions in the nanomolar concentration range. The quenching of the PL intensity of the nanocluster by Ag(I) can be attributed to the conversion of atomically precise nanocluster to nanoparticles thereby losing its energy quantization. The quenching mechanism can be explained by both static and dynamic process as indicated by the lifetime measurements which was in agreement with the PL intensity based Stern-Volmer plot. On-site visual detection of Ag(I) was also achieved with portable paper strips coated with Trp-Cu NC. The excellent biocompatibility of the nanocluster was confirmed from the cell viability studies. Small tryptophan molecule as a scaffold allowed the nanocluster to easily penetrate the cell membrane, thus it was successfully used as a bio-marker for live-cell imaging making it a promising candidate for in-vivo studies as an intracellular sensor. Significant spectral overlap with an anticancer drug (doxorubicin) allows it to be used as a FRET pair adding further value to its features. Overall, the synthesized Trp-Cu nanocluster can be used as an excellent nano-sensor for Ag(I) detection, bio-imaging, in-vivo studies and can also be potentially extended for various theragnostic applications.

Acknowledgement

S.S.M. thanks SERB, Government of India (Project no. SRG/2020/001710) and IIT Palakkad for financial assistance. B.R.S thanks SERB, Government of India (Project no. ECR/2016/001986) for financial support. A. thanks UGC, Government of India and T.T. thanks SERB, Government of India (Project no. SRG/2020/001710) for providing fellowships. S.S.M. thanks the central instrumentation facility (CIF) IIT Palakkad for FTIR measurements, CIF IISER Trivandrum for MALDI-TOF and XPS measurements, Dr. Pratik Sen, IIT Kanpur for lifetime measurements, SCIF SRM institute of Science and Technology for TEM measurements and IIT Madras for ICP-OES measurements.

Declarations

Competing interests: The authors declare no competing interests

REFERENCES

1. Lu Y, Chen W (2012) Sub-nanometre sized metal clusters: from synthetic challenges to the unique property discoveries. Chem Soc Rev 41:3594–3623. https://doi.org/10.1039/C2CS15325D

2. Baghdasaryan A, Bürgi T (2021) Copper nanoclusters: designed synthesis, structural diversity, and multiplatform applications. Nanoscale 13:6283–6340. https://doi.org/10.1039/D0NR08489A

3. Meng X, Zare I, Yan X, Fan K (2020) Protein-protected metal nanoclusters: An emerging ultra-small nanozyme. WIREs Nanomedicine Nanobiotechnology 12:. https://doi.org/10.1002/wnan.1602

4. Lin Z, Goswami N, Xue T, et al (2021) Engineering Metal Nanoclusters for Targeted Therapeutics: From Targeting Strategies to Therapeutic Applications. Adv Funct Mater 31:2105662. https://doi.org/10.1002/adfm.202105662

5. Liu W, Wang J, Yuan S, et al (2021) Chiral Superatomic Nanoclusters Ag_{47} Induced by the Ligation of Amino Acids. Angew Chem Int Ed 60:11430–11435. https://doi.org/10.1002/anie.202100972

6. Xie J, Zheng Y, Ying JY (2009) Protein-Directed Synthesis of Highly Fluorescent Gold Nanoclusters. J Am Chem Soc 131:888–889. https://doi.org/10.1021/ja806804u

7. Xavier PL, Chaudhari K, Baksi A, Pradeep T (2012) Protein-protected luminescent noble metal quantum clusters: an emerging trend in atomic cluster nanoscience. Nano Rev 3:10.3402/nano.v3i0.14767. https://doi.org/10.3402/nano.v3i0.14767

8. Rajamanikandan R, Ilanchelian M (2019) Red emitting human serum albumin templated copper nanoclusters as effective candidates for highly specific biosensing of bilirubin. Mater Sci Eng C 98:1064–1072. https://doi.org/10.1016/j.msec.2019.01.048

9. Krishna Kumar AS, Tseng W-L (2020) Perspective on recent developments of near infrared-emitting gold nanoclusters: applications in sensing and bio-imaging. Anal Methods 12:1809–1826. https://doi.org/10.1039/D0AY00157K

10. Wen F, Dong Y, Feng L, et al (2011) Horseradish Peroxidase Functionalized Fluorescent Gold Nanoclusters for Hydrogen Peroxide Sensing. Anal Chem 83:1193–1196. https://doi.org/10.1021/ac1031447

11. Ramadurai M, Rajendran G, Bama TS, et al (2020) Biocompatible thiolate protected copper nanoclusters for an efficient imaging of lung cancer cells. J Photochem Photobiol B 205:111845. https://doi.org/10.1016/j.jphotobiol.2020.111845

12. Shahsavari S, Hadian-Ghazvini S, Hooriabad Saboor F, et al (2019) Ligand functionalized copper nanoclusters for versatile applications in catalysis, sensing, bioimaging, and optoelectronics. Mater Chem Front 3:2326–2356. https://doi.org/10.1039/C9QM00492K

13. Zare I, Chevrier DM, Cifuentes-Rius A, et al (2021) Protein-protected metal nanoclusters as diagnostic and therapeutic platforms for biomedical applications. Mater Today S1369702120303825. https://doi.org/10.1016/j.mattod.2020.10.027

14. Lai W-F, Wong W-T, Rogach AL (2020) Development of Copper Nanoclusters for In Vitro and In Vivo Theranostic Applications. Adv Mater 32:1906872. https://doi.org/10.1002/adma.201906872

15. Benavides J, Quijada-Garrido I, García O (2020) The synthesis of switch-off fluorescent water-stable copper nanocluster Hg^{2+} sensors *via* a simple one-pot approach by an *in situ* metal reduction strategy in the presence of a thiolated polymer ligand template. Nanoscale 12:944–955. https://doi.org/10.1039/C9NR08439H

16. Song X-R, Goswami N, Yang H-H, Xie J (2016) Functionalization of metal nanoclusters for biomedical applications. The Analyst 141:3126–3140. https://doi.org/10.1039/C6AN00773B

17. Bhattacharyya K, Mukherjee S (2018) Fluorescent Metal Nano-Clusters as Next Generation Fluorescent Probes for Cell Imaging and Drug Delivery. Bull Chem Soc Jpn 91:447–454. https://doi.org/10.1246/bcsj.20170377

18. Ghosh S, Das NK, Anand U, Mukherjee S (2015) Photostable Copper Nanoclusters: Compatible Förster Resonance Energy-Transfer Assays and a Nanothermometer. J Phys Chem Lett 6:1293–1298. https://doi.org/10.1021/acs.jpclett.5b00378

19. Akhuli A, Preeyanka N, Chakraborty D, Sarkar M (2022) Turn-Off Detection of Reactive Oxidative Species and Turn-On Detection of Antioxidants Using Fluorescent Copper Nanoclusters. ACS Appl Nano Mater 5:5826–5837. https://doi.org/10.1021/acsanm.2c01005

20. Chakraborty S, Mukherjee S (2021) Role of Small Moiety of a Large Ligand: Tyrosine Templated Copper Nanoclusters. J Phys Chem Lett 12:3266–3273. https://doi.org/10.1021/acs.jpclett.1c00245

21. Saleh SM, El-Sayed WA, El-Manawaty MA, et al (2022) Microwave-Assisted Rapid Synthesis of Luminescent Tryptophan-Stabilized Silver Nanoclusters for Ultra-Sensitive Detection of Fe(III), and Their Application in a Test Strip. Biosensors 12:425. https://doi.org/10.3390/bios12060425

22. Mosquera J, García I, Liz-Marzán LM (2018) Cellular Uptake of Nanoparticles versus Small Molecules: A Matter of Size. Acc Chem Res 51:2305–2313. https://doi.org/10.1021/acs.accounts.8b00292

23. Richard DM, Dawes MA, Mathias CW, et al (2009) L-Tryptophan: Basic Metabolic Functions, Behavioral Research and Therapeutic Indications. Int J Tryptophan Res IJTR 2:45–60. https://doi.org/10.4137/ijtr.s2129

24. Paredes SD, Barriga C, Reiter RJ, Rodríguez AB (2009) Assessment of the Potential Role of Tryptophan as the Precursor of Serotonin and Melatonin for the Aged Sleep-wake Cycle and Immune Function: Streptopelia Risoria as a Model. Int J Tryptophan Res IJTR 2:23–36. https://doi.org/10.4137/ijtr.s1129

25. Fukuwatari T, Shibata K (2013) Nutritional aspect of tryptophan metabolism. Int J Tryptophan Res IJTR 6:3–8. https://doi.org/10.4137/IJTR.S11588

26. Gasperi V, Sibilano M, Savini I, Catani MV (2019) Niacin in the Central Nervous System: An Update of Biological Aspects and Clinical Applications. Int J Mol Sci 20:E974. https://doi.org/10.3390/ijms20040974

27. de Jesus AJ, Allen TW (2013) The role of tryptophan side chains in membrane protein anchoring and hydrophobic mismatch. Biochim Biophys Acta BBA - Biomembr 1828:864–876. https://doi.org/10.1016/j.bbamem.2012.09.009

28. Khemaissa S, Sagan S, Walrant A (2021) Tryptophan, an Amino-Acid Endowed with Unique Properties and Its Many Roles in Membrane Proteins. Crystals 11:1032. https://doi.org/10.3390/cryst11091032

29. Sim W, Barnard R, Blaskovich MAT, Ziora Z (2018) Antimicrobial Silver in Medicinal and Consumer Applications: A Patent Review of the Past Decade (2007–2017). Antibiotics 7:93. https://doi.org/10.3390/antibiotics7040093

30. Prasher P, Sharma M, Mudila H, et al (2020) Emerging trends in clinical implications of bio-conjugated silver nanoparticles in drug delivery. Colloid Interface Sci Commun 35:100244. https://doi.org/10.1016/j.colcom.2020.100244

31. Windler L, Height M, Nowack B (2013) Comparative evaluation of antimicrobials for textile applications. Environ Int 53:62–73. https://doi.org/10.1016/j.envint.2012.12.010

32. Sharma RK, Yadav S, Dutta S, et al (2021) Silver nanomaterials: synthesis and (electro/photo) catalytic applications. Chem Soc Rev 50:11293–11380. https://doi.org/10.1039/D0CS00912A

33. Chen D, Qiao X, Qiu X, Chen J (2009) Synthesis and electrical properties of uniform silver nanoparticles for electronic applications. J Mater Sci 44:1076–1081. https://doi.org/10.1007/s10853-008-3204-y

34. Mijnendonckx K, Leys N, Mahillon J, et al (2013) Antimicrobial silver: uses, toxicity and potential for resistance. BioMetals 26:609–621. https://doi.org/10.1007/s10534-013-9645-z

35. Ratte HT (1999) Bioaccumulation and toxicity of silver compounds: A review. Environ Toxicol Chem 18:89–108. https://doi.org/10.1002/etc.5620180112

36. Lansdown ABG (2010) A Pharmacological and Toxicological Profile of Silver as an Antimicrobial Agent in Medical Devices. Adv Pharmacol Sci 2010:1–16. https://doi.org/10.1155/2010/910686

37. Hadrup N, Sharma AK, Loeschner K (2018) Toxicity of silver ions, metallic silver, and silver nanoparticle materials after in vivo dermal and mucosal surface exposure: A review. Regul Toxicol Pharmacol 98:257–267. https://doi.org/10.1016/j.yrtph.2018.08.007

38. Mota L, Dinis-Oliveira RJ (2021) Clinical and Forensic Aspects of the Different Subtypes of Argyria. J Clin Med 10:2086. https://doi.org/10.3390/jcm10102086

39. Huy GD, Zhang M, Zuo P, Ye B-C (2011) Multiplexed analysis of silver(i) and mercury(ii) ions using oligonucletide–metal nanoparticle conjugates. The Analyst 136:3289. https://doi.org/10.1039/c1an15373k

40. Gordon O, Vig Slenters T, Brunetto PS, et al (2010) Silver Coordination Polymers for Prevention of Implant Infection: Thiol Interaction, Impact on Respiratory Chain Enzymes, and Hydroxyl Radical Induction. Antimicrob Agents Chemother 54:4208–4218. https://doi.org/10.1128/AAC.01830-09

41. Jiravova J, Tomankova KB, Harvanova M, et al (2016) The effect of silver nanoparticles and silver ions on mammalian and plant cells in vitro. Food Chem Toxicol 96:50–61. https://doi.org/10.1016/j.fct.2016.07.015

42. Arulraj AD, Devasenathipathy R, Chen S-M, et al (2015) Highly selective and sensitive fluorescent chemosensor for femtomolar detection of silver ion in aqueous medium. Sens Bio-Sens Res 6:19–24. https://doi.org/10.1016/j.sbsr.2015.10.004

43. Li B, Du Y, Dong S (2009) DNA based gold nanoparticles colorimetric sensors for sensitive and selective detection of Ag(I) ions. Anal Chim Acta 644:78–82. https://doi.org/10.1016/j.aca.2009.04.022

44. Dalmieda J, Zubiarrain-Laserna A, Ganepola D, et al (2021) Chemiresistive detection of silver ions in aqueous media. Sens Actuators B Chem 328:129023. https://doi.org/10.1016/j.snb.2020.129023

45. Mohammadi SZ, Afzali D, Heshmati Z (2013) Ligand-less *in situ* surfactant-based solid phase extraction for preconcentration of silver from natural water samples prior to its determination by atomic absorption spectroscopy. Toxicol Environ Chem 95:1299–1308. https://doi.org/10.1080/02772248.2014.881829

46. Poitras EP, Levine MA, Harrington JM, et al (2015) Development of an Analytical Method for Assessment of Silver Nanoparticle Content in Biological Matrices by Inductively Coupled Plasma Mass Spectrometry. Biol Trace Elem Res 163:184–192. https://doi.org/10.1007/s12011-014-0141-2

47. Clark NJ, Clough R, Boyle D, Handy RD (2019) Development of a suitable detection method for silver nanoparticles in fish tissue using single particle ICP-MS. Environ Sci Nano 6:3388–3400. https://doi.org/10.1039/C9EN00547A

48. Guo H, Xing B, Hamlet LC, et al (2016) Surface-enhanced Raman scattering detection of silver nanoparticles in environmental and biological samples. Sci Total Environ 554–555:246–252. https://doi.org/10.1016/j.scitotenv.2016.02.084

49. Zhou M, Lin T, Gan X (2017) Colorimetric aggregation assay for silver(I) based on the use of aptamer modified gold nanoparticles and C-Ag(I)-C interaction. Microchim Acta 184:4671–4677. https://doi.org/10.1007/s00604-017-2518-3

50. Carter KP, Young AM, Palmer AE (2014) Fluorescent Sensors for Measuring Metal Ions in Living Systems. Chem Rev 114:4564–4601. https://doi.org/10.1021/cr400546e

51. Li L, Wang J, Xu S, et al (2022) Recent Progress in Fluorescent Probes For Metal Ion Detection. Front Chem 10:875241. https://doi.org/10.3389/fchem.2022.875241

52. Liu Y, Liu Y, Li Z, et al (2015) An unusual red-to-brown colorimetric sensing method for ultrasensitive silver(I) ion detection based on a non-aggregation of hyperbranched polyethylenimine derivative stabilized gold nanoparticles. The Analyst 140:5335–5343. https://doi.org/10.1039/C5AN00932D

53. Liao S, Zhao X, Zhu F, et al (2018) Novel S, N-doped carbon quantum dot-based "off-on" fluorescent sensor for silver ion and cysteine. Talanta 180:300–308. https://doi.org/10.1016/j.talanta.2017.12.040

54. Wang F, Lu Y, Chen Y, et al (2018) Colorimetric Nanosensor Based on the Aggregation of AuNP Triggered by Carbon Quantum Dots for Detection of Ag^{+} Ions. ACS Sustain Chem Eng 6:3706–3713. https://doi.org/10.1021/acssuschemeng.7b04067

55. Cui W, Wang L, Xiang G, et al (2015) A colorimetric and fluorescence "turn-off" chemosensor for the detection of silver ion based on a conjugated polymer containing 2,3-di(pyridin-2-yl)quinoxaline. Sens Actuators B Chem 207:281–290. https://doi.org/10.1016/j.snb.2014.10.072

56. Kang J, Choi M, Kwon JY, et al (2002) New Fluorescent Chemosensors for Silver Ion. J Org Chem 67:4384–4386. https://doi.org/10.1021/jo020123x

57. Shiohara A, Hoshino A, Hanaki K-I, et al (2004) On the cyto-toxicity caused by quantum dots. Microbiol Immunol 48:669–675. https://doi.org/10.1111/j.1348-0421.2004.tb03478.x

58. Hu Y-L, Liu A-Y, Wu B-C, et al (2021) Modulating fluorescence emission of l-methionine-stabilized Au nanoclusters from green to red and its application for visual detection of silver ion. Microchem J 166:106198. https://doi.org/10.1016/j.microc.2021.106198

59. Kang J, Gao P, Zhang G, et al (2022) Rapid sonochemical synthesis of copper nanoclusters with red fluorescence for highly sensitive detection of silver ions. Microchem J 178:107370. https://doi.org/10.1016/j.microc.2022.107370

60. An M, Li H, Su M, et al (2021) Cu2+ enhanced fluorescent Ag nanoclusters with tunable emission from red to yellow and the application for Ag+ sensing. Spectrochim Acta A Mol Biomol Spectrosc 252:119484. https://doi.org/10.1016/j.saa.2021.119484

61. Wang J, Liu A-Y, Wu B-C, et al (2021) Highly selective and rapid detection of silver ions by using a "turn on" non-fluorescent cysteine stabilized gold nanocluster probe. Anal Methods 13:2099–2106. https://doi.org/10.1039/D1AY00241D

62. Kardar ZS, Shemirani F, Zadmard R (2020) Determination of iron(II) and iron(III) via static quenching of the fluorescence of tryptophan-protected copper nanoclusters. Microchim Acta 187:81. https://doi.org/10.1007/s00604-019-4067-4

63. Sebastian A, Aarya, Sarangi BR, Sen Mojumdar S (2023) Lysozyme protected copper nano-cluster: A photo-switch for the selective sensing of Fe2+. J Photochem Photobiol Chem 436:114378. https://doi.org/10.1016/j.jphotochem.2022.114378

64. Principles of Fluorescence Spectroscopy | Joseph R. Lakowicz | Springer. https://www.springer.com/gp/book/9780387312781. Accessed 17 Apr 2020

65. Anusuyadevi K, Wu SP, Velmathi S (2021) Reversible enhancement of fluorescence in acidic pH driven by tryptophan stabilized copper nanoclusters and its application in bioimaging. J Photochem Photobiol Chem 421:113526. https://doi.org/10.1016/j.jphotochem.2021.113526

66. Zhao X, Zhao RG, Yang WS (2002) Self-Assembly of l-Tryptophan on the Cu(001) Surface. Langmuir 18:433–438. https://doi.org/10.1021/la010542+

67. Zhang P, Chan W, Ang IL, et al (2019) Revisiting Fragmentation Reactions of Protonated α-Amino Acids by High-Resolution Electrospray Ionization Tandem Mass Spectrometry with Collision-Induced Dissociation. Sci Rep 9:6453. https://doi.org/10.1038/s41598-019-42777-8

68. Domingues MRM, Domingues P, Reis A, et al (2003) Identification of oxidation products and free radicals of tryptophan by mass spectrometry. J Am Soc Mass Spectrom 14:406–416. https://doi.org/10.1016/S1044-0305(03)00127-2

69. Zheng J, Nicovich PR, Dickson RM (2007) Highly Fluorescent Noble-Metal Quantum Dots. Annu Rev Phys Chem 58:409–431. https://doi.org/10.1146/annurev.physchem.58.032806.104546

70. Zheng J, Zhang C, Dickson RM (2004) Highly Fluorescent, Water-Soluble, Size-Tunable Gold Quantum Dots. Phys Rev Lett 93:077402. https://doi.org/10.1103/PhysRevLett.93.077402

71. Sarkar P, Saha M, Nandi N, et al (2022) Red-Emitting Silver Nanoclusters for Dual-Mode Detection of Cu^{2+} and Vitamin B_{12} in Living Cells. ACS Appl Nano Mater 5:7670–7678. https://doi.org/10.1021/acsanm.1c04496

72. Das NK, Mukherjee S (2018) Size-controlled atomically precise copper nanoclusters: Synthetic protocols, spectroscopic properties and applications. Phys Sci Rev 3:. https://doi.org/10.1515/psr-2017-0081

73. Mátyus L, Szöllősi J, Jenei A (2006) Steady-state fluorescence quenching applications for studying protein structure and dynamics. J Photochem Photobiol B 83:223–236. https://doi.org/10.1016/j.jphotobiol.2005.12.017

74. Doherty GJ, McMahon HT (2009) Mechanisms of endocytosis. Annu Rev Biochem 78:857–902. https://doi.org/10.1146/annurev.biochem.78.081307.110540

75. Ha T (2001) Single-molecule fluorescence resonance energy transfer. Methods San Diego Calif 25:78–86. https://doi.org/10.1006/meth.2001.1217

76. Stryer L (1978) Fluorescence energy transfer as a spectroscopic ruler. Annu Rev Biochem 47:819–846. https://doi.org/10.1146/annurev.bi.47.070178.004131

77. Schuler B, Eaton WA (2008) Protein folding studied by single-molecule FRET. Curr Opin Struct Biol 18:16–26. https://doi.org/10.1016/j.sbi.2007.12.003

78. Dey D, Saha J, Roy AD, et al (2014) Sensing of DNA conformation based on change in FRET efficiency between laser dyes. Sens Actuators B Chem 204:746–753. https://doi.org/10.1016/j.snb.2014.08.029

79. Wijesinghe KM, Kanak MA, Harrell JC, Dhakal S (2022) Single-Molecule Sensor for High-Confidence Detection of miRNA. ACS Sens 7:1086–1094. https://doi.org/10.1021/acssensors.1c02748

80. Xiao Y, Shu F, Wong K-Y, Liu Z (2013) Förster resonance energy transfer-based biosensing platform with ultrasmall silver nanoclusters as energy acceptors. Anal Chem 85:8493–8497. https://doi.org/10.1021/ac402125g

TABLE AND FIGURES

Table 1: Recovery of Ag(I) from different complex systems.

Sample	Concentration of Ag (I) added	Concentration of Ag (I) recovered	Concentration of Ag(I) obtained from ICP-OES method
Tap water	500 nM	553 ± 190 nM	760 nM
	50 µM	57.36 ± 12 µM	49.56 µM
	100 µM	85.6 ± 4 µM	94.65 µM
Human Blood Serum	500 nM	586 ± 123 nM	611.9 nM
	50 µM	53.22 ± 6 µM	51.9 µM
	100 µM	89.86 ± 4 µM	104.49 µM

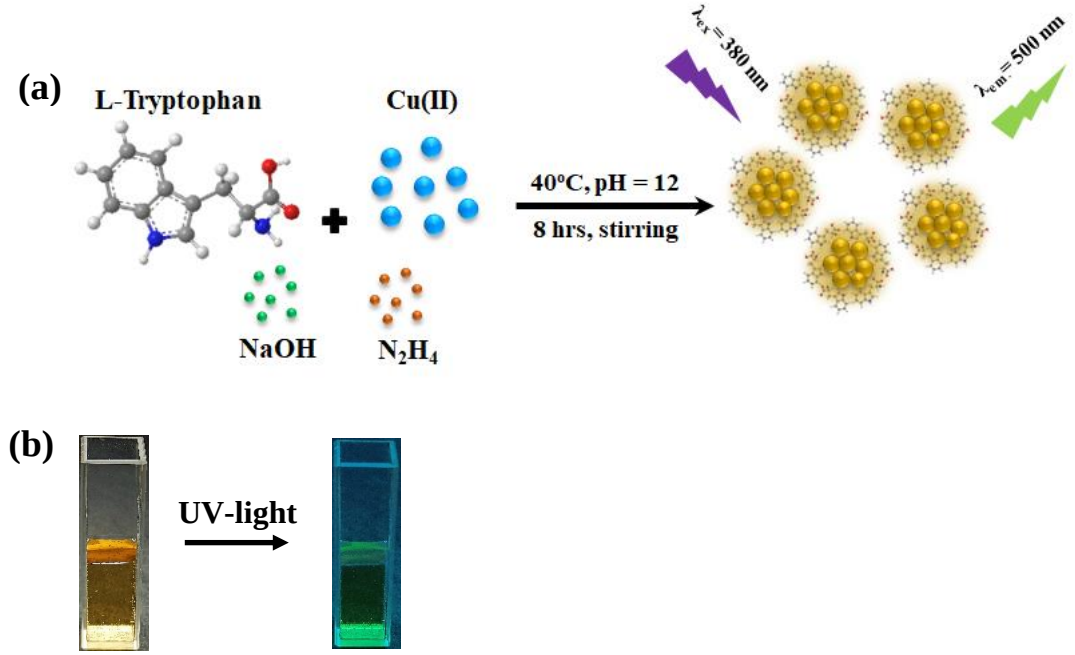

Scheme 1: (a) Schematic representation of synthesis of Trp-Cu nanocluster. **(b)** Trp-Cu nanocluster under visible light (yellowish brown) and ultra-violet (UV) light (green).

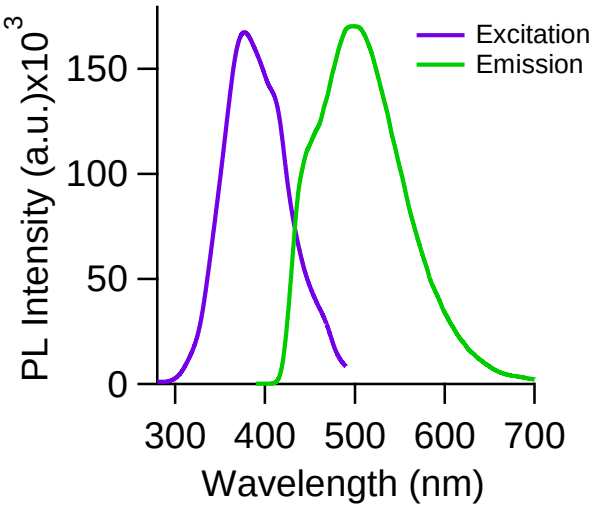

Figure 1: Emission (λ_{ex} = 380 nm) and excitation (λ_{em} = 500 nm) spectra of Trp-Cu NC.

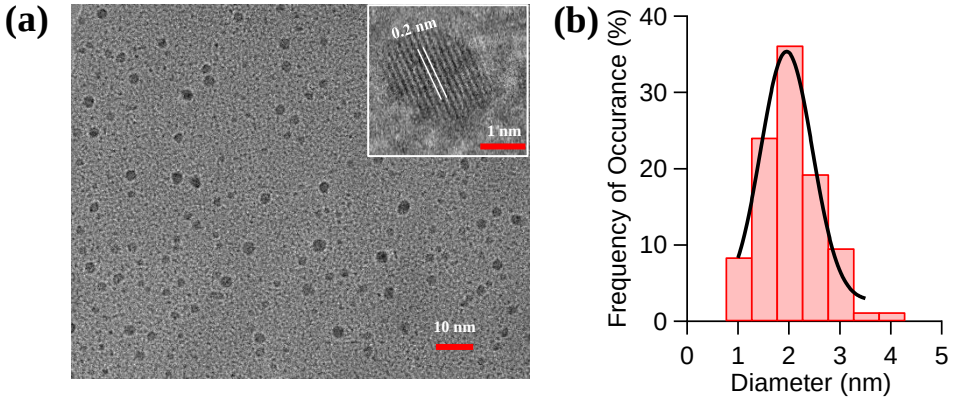

Figure 2: (a) Transmission electron microscope (TEM) image of Trp-Cu NC confirming the formation of ultrasmall spherical clusters. The lattice fringes are also visible (inset). **(b)** Size distribution of the nanocluster obtained from the TEM image showing an average size of ~2 nm.

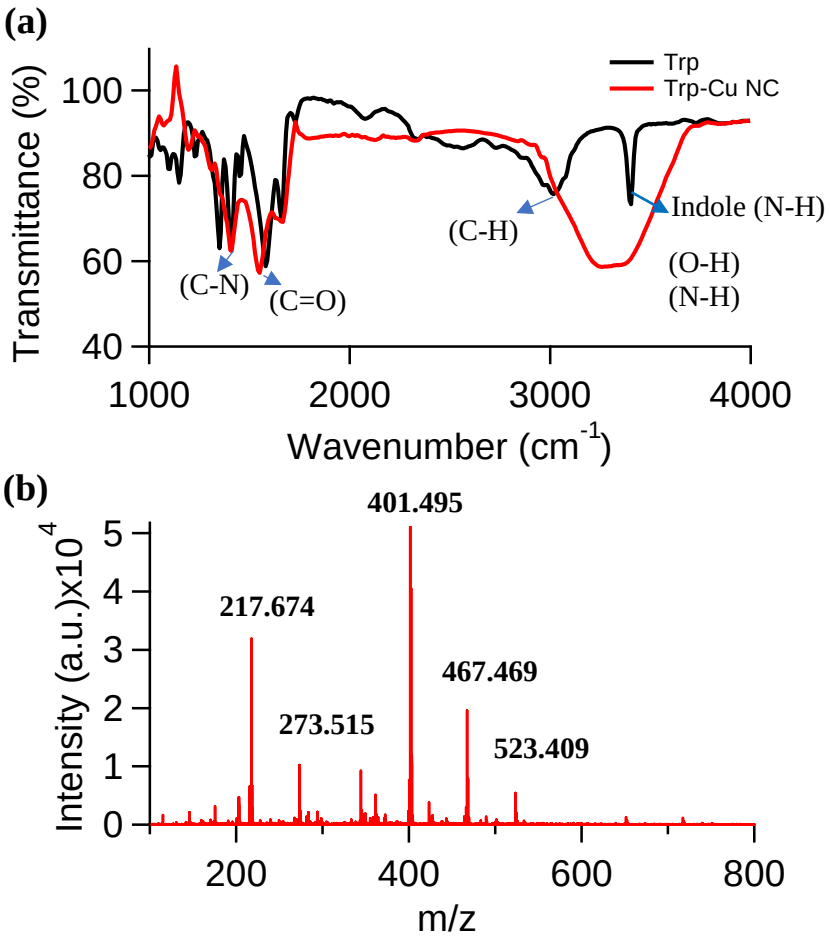

Figure 3: (a) FTIR spectra of tryptophan (black) and Trp-Cu NC (red). (b) MALDI-TOF mass spectrum of Trp-Cu NC.

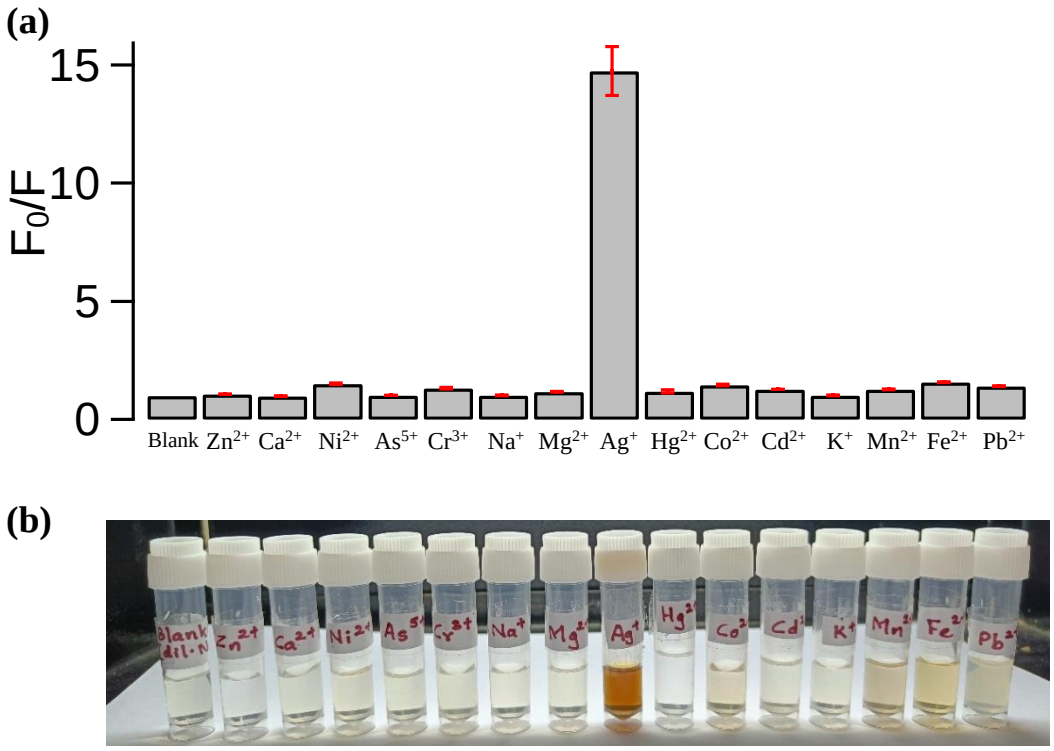

Figure 4: (a) Ratio of PL intensity of Trp-Cu NC in the absence (F_0) and presence of Ag(I) (~200 μM) and different other metal ions (~500 μM) (F) showing selective detection of Ag(I). **(b)** Colour change of the diluted nanocluster can be visualised upon addition of Ag(I) compared to other metal ions (~500 μM).

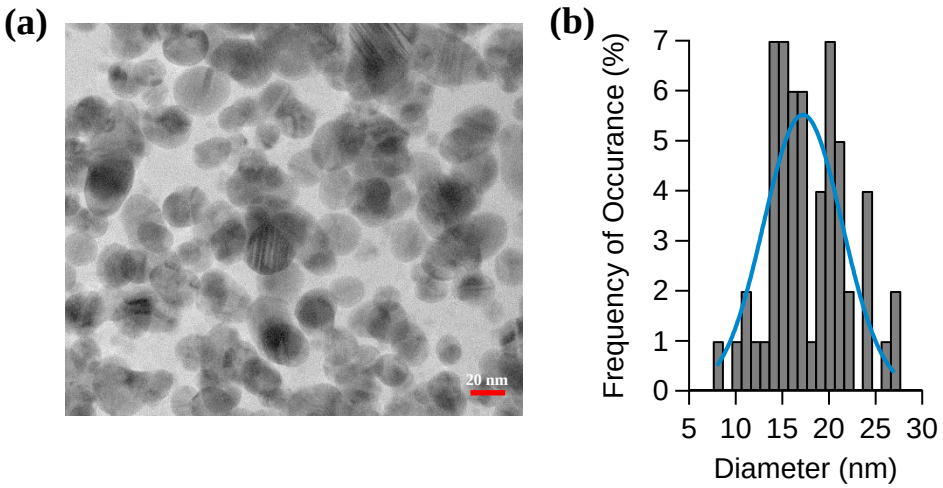

Figure 5: (a) Transmission electron microscope (TEM) image of Trp-Cu NC in the presence of 500 μM Ag(I). **(b)** The size distribution of the nanocluster in the presence of Ag(I).

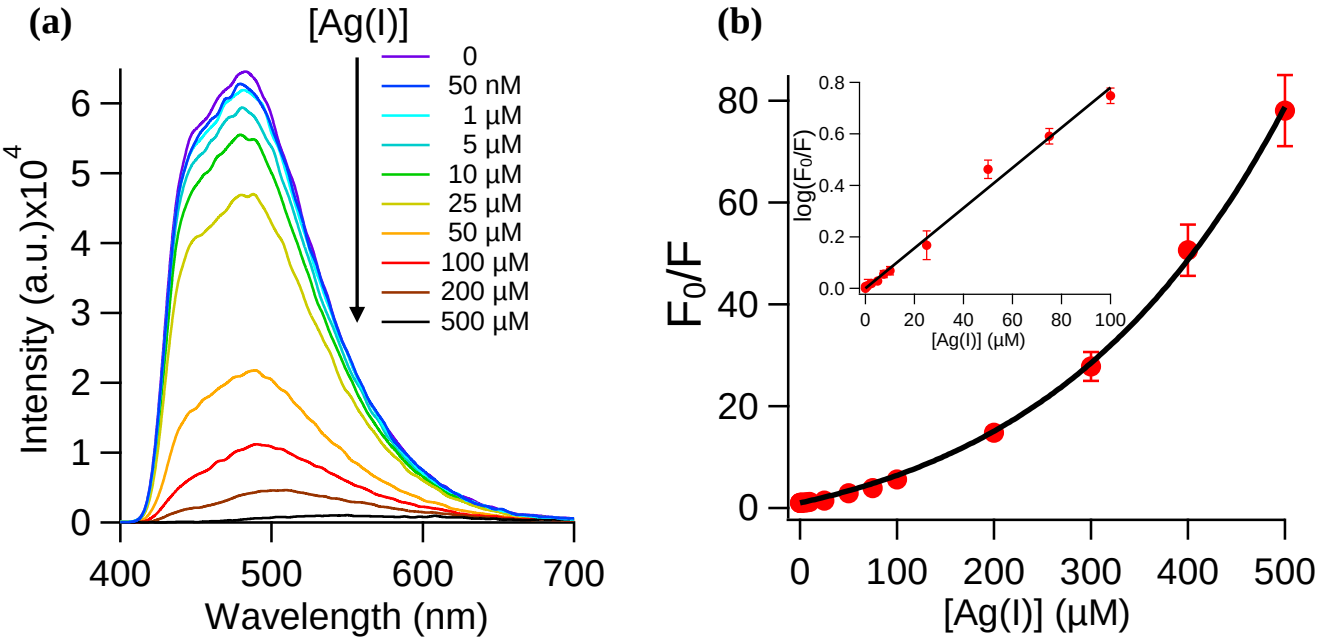

Figure 6: (a) PL intensity of Trp-Cu NC gradually quenched with increasing concentration of Ag(I). **(b)** Corresponding Stern-Volmer plot showing upward curvature. The black line represents a fit using equation 1 with both static and dynamic quenching contributions. Inset represents a plot of log(F_0/F) vs [Ag(I)] (red) with a linear fit (black).

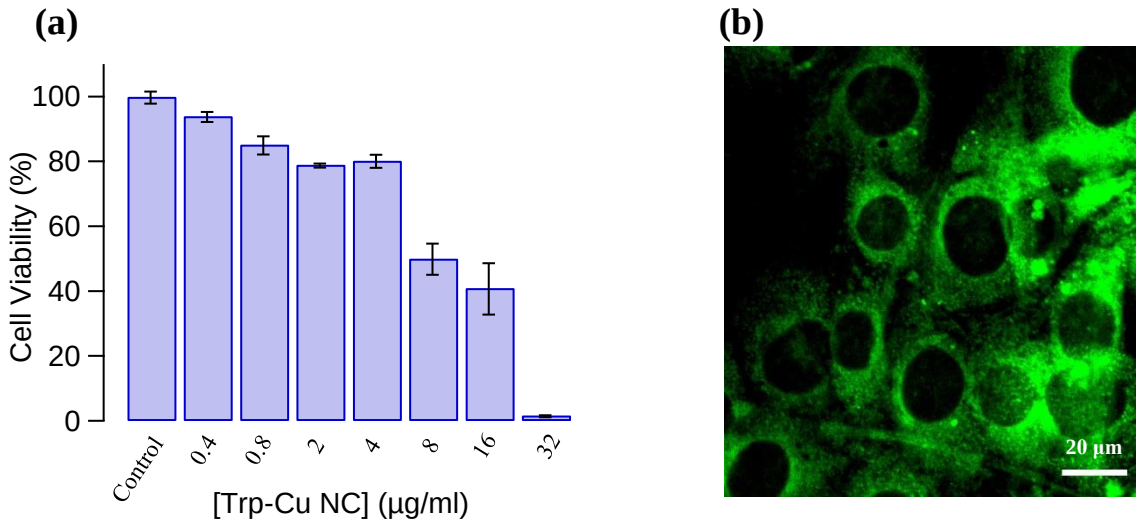

Figure 7: (a) The cell viability assay showing that the nanocluster is not cytotoxic to the 3T3 cells. **(b)** Confocal microscope image of 3T3 cells incubated with Trp-Cu NC (λ_{ex} = 405 nm).

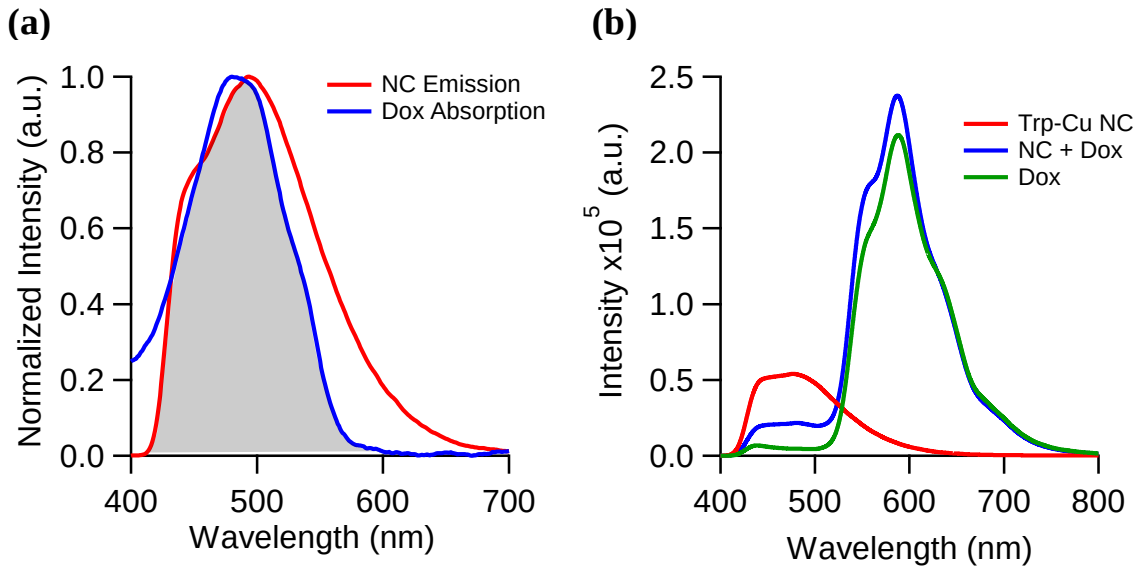

Figure 8: (a) Spectral overlap between normalized emission spectra (λ_{ex} = 380 nm) of the Trp-Cu nanocluster (donor) (red) and the absorption spectra of doxorubicin (acceptor) (blue). **(b)** Emission spectra (λ_{ex} = 380 nm) of 100 μM doxorubicin (acceptor) (green), the nanocluster (donor) in the absence (red) and presence of 100 μM doxorubicin (blue).